Recent results on soft QCD topics from ATLAS

Roman Lysák[*†]

Institute of Physics of the Czech Academy of Sciences, Prague
E-mail: lysak@fzu.cz

The paper presents various soft QCD related measurements performed by the ATLAS Collaboration at the LHC using early Run 2 proton-proton collisions at a centre-of-mass energy of $\sqrt{s} = 13$ TeV as well as Run 1 data at $\sqrt{s} = 7$ TeV. The paper covers the measurements of total, elastic and inelastic proton-proton cross-sections. The measurement of the charged-particle production and the measurement of the distributions sensitive to underlying event are also presented. Finally, the diffractive dijet production and the exclusive $\gamma + \gamma \to \ell\ell$ production are described.

54th International Winter Meeting on Nuclear Physics
25-29 January 2016
Bormio, Italy

---

[*]Speaker.

[†]On behalf of the ATLAS Collaboration

1. Introduction

In a typical proton-proton (pp) collision, there is hard interaction which can be calculated perturbatively in quantum chromodynamics (QCD), but there are also soft components of the event for which only phenomenological models exist. These soft components are, for example, the multi-parton interactions, the beam remnants, the initial and final state radiations, and the hadronization of partons producing the final state particles. Measuring the processes sensitive to such soft QCD effects helps to constrain parameters of the phenomenological models. Although the main objective of the ATLAS experiment is to study the Higgs boson and search for physics beyond the Standard Model, understanding well the effect of soft QCD is important and has direct impact on such measurements. The reason is that soft QCD results are applied to tune the Monte Carlo (MC) generators which are consequently used e.g. for the simulation of the multiple proton-proton interactions (pile-up) in any MC simulation in the ATLAS experiment.

The new LHC data taking, Run 2, started in 2015 at the pp centre-of-mass energy $\sqrt{s} = 13$ TeV. There are two ATLAS detector [1] components which were changed before Run 2 and are important for the measurements presented here: the rebuild of the scintillator detectors (MBTS) used for triggering of the events in the forward region and the addition of a pixel detector layer (IBL) closest to the beamline to improve the reconstruction of charged tracks.

2. The total, elastic, and inelastic pp cross-section

The total hadronic cross-section is a basic property of strong interactions, but it cannot be calculated from the first principles yet, since the evaluation of all soft QCD effects is involved. It was extracted from elastic scattering data at $\sqrt{s} = 7$ TeV [2] using the optical theorem. An extrapolation of the differential elastic cross-section to $|t| \to 0$, where t is the four-momentum transfer, gives the total cross-section through the formula:

$$\sigma_{\text{tot}}^2 = \frac{16\pi(\hbar c)^2}{1+\rho^2} \left. \frac{d\sigma_{\text{el}}}{dt} \right|_{t \to 0},$$
(2.1)

where ρ is a small correction coming from the ratio of the real to imaginary part of the elastic scattering amplitude in the forward direction and is extracted from global fits performed by the COMPETE Collaboration to lower-energy elastic-scattering data.

The ALFA Roman pot detectors located about 240 m away from the main ATLAS detector were used for this measurement, see Fig. 1. The low-luminosity run with clean conditions and special beam optics were used. By reconstructing the scattering angle θ^*, the four-momentum transfer t is calculated as $-t = (\theta^* \times p)^2$ where p is the nominal beam momentum of the LHC of 3.5 TeV. The elastic cross-section as a function of momentum transfer t is determined using an independent method to measure data luminosity with a precision of 2.3%. The fit of $t-$spectrum was performed using a theoretical formula, see Fig. 2. The measured total cross-section is $\sigma_{\text{tot}} = 95.35 \pm 0.38(stat) \pm 1.25(exp) \pm 0.37(extr)$ mb and the nuclear slope characterizing the nuclear term of the theoretical formula is $B = 19.73 \pm 0.14(stat) \pm 0.26(syst)$ GeV^{-2}. The dominant systematic uncertainties for the total cross-section measurement are due to luminosity uncertainty, the beam energy uncertainty and the reconstruction efficiency uncertainty. For B, the experimental systematic uncertainty is dominated by the beam energy uncertainty.
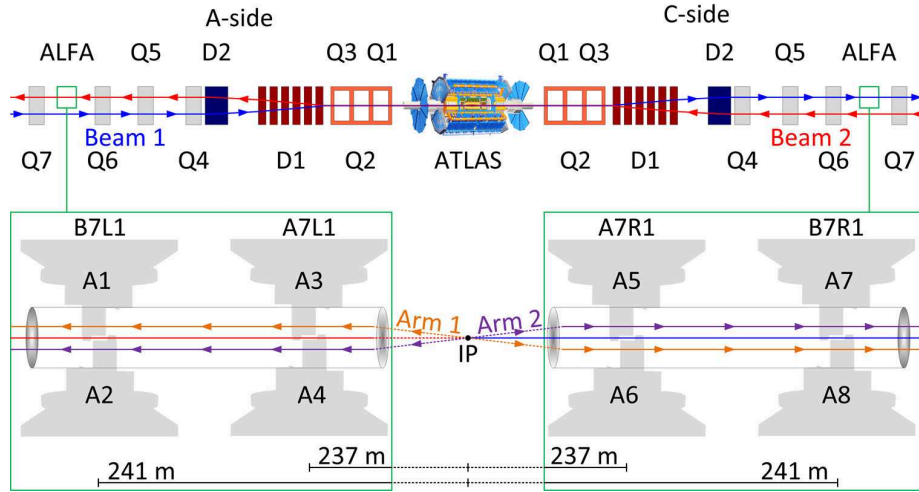
Figure 1: A sketch of the experimental set-up, not to scale, showing the positions of the ALFA Roman Pot stations in the outgoing LHC beams [2].
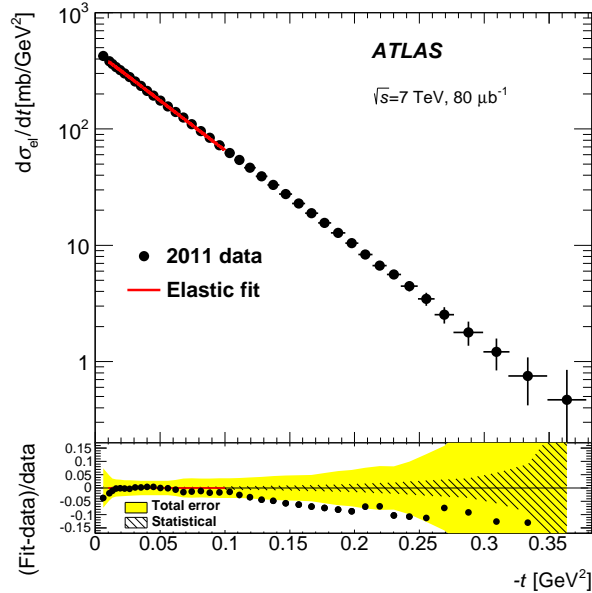

Figure 2: A fit of the theoretical prediction with σ_{tot} and B as free parameters to the differential elastic cross-section [2].

The total elastic cross-section is then estimated by integrating the parameterized form of the differential elastic cross section which includes just the nuclear term:

$$\frac{d\sigma_{el}}{dt} = \frac{d\sigma_{el}}{dt}\bigg|_{t\to 0} \exp(-B|t|) \qquad \text{with} \qquad \frac{d\sigma_{el}}{dt}\bigg|_{t\to 0} = \sigma_{tot}^2 \frac{1+\rho^2}{16\pi(\hbar c)^2}. \qquad (2.2)$$

It is measured to be $\sigma_{el} = 24.00 \pm 0.19(stat) \pm 0.57(syst)$ mb. The inelastic cross-section is determined indirectly by subtracting the elastic cross-section from the total cross-section and it is $\sigma_{inel} = 71.34 \pm 0.36(stat) \pm 0.83(syst)$ mb.
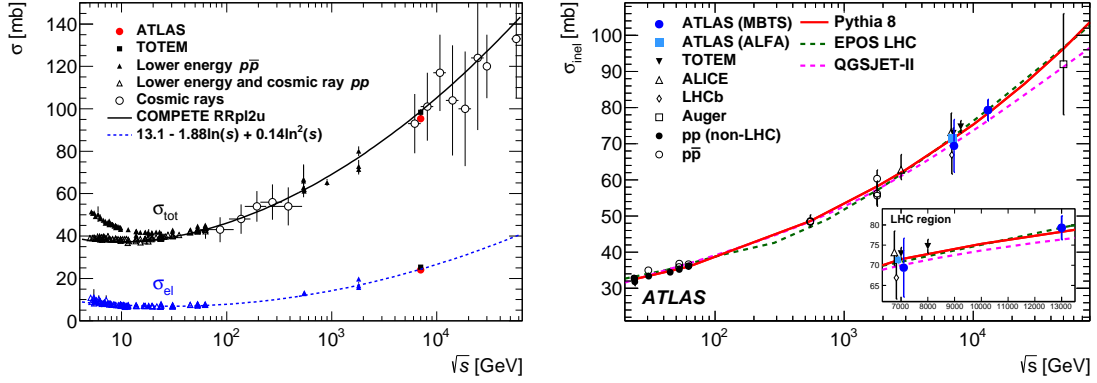
Figure 3: Left, the comparison of total and elastic cross-section measurements presented here with other published measurements and model predictions as a function of the centre-of-mass energy [2]. Right, the inelastic proton-proton cross-section versus $\sqrt{s}$ [5].

Figure 3 shows the comparison of this measurement to other measurements at different energies and to model predictions for all three (total, elastic and inelastic) cross-sections. The ATLAS measurement of the total cross-section is about two standard deviations (2σ) below the COMPETE parametrization [3] and a little bit smaller ($\sim 1.3\sigma$) compared to the measurement by TOTEM [4].

A direct measurement of the inelastic cross-section has been already performed in Run 2 at $\sqrt{s} = 13$ TeV [5]. It is achieved by using MBTS positioned well enough in the forward region ($2.07 < |\eta| < 3.86$) to detect the inelastic collisions but not the elastic ones.

The largest rapidity gap between any two hadrons is used to define the boundary between two collections of hadrons (the dissociation systems). The measurement is performed in the fiducial region requiring that the largest invariant mass (M_X) of one of the dissociation systems is $\xi = M_X^2/s > 10^{-6}$.

Two selections with different requirements on hits in MBTS are applied to constrain the normalization of diffraction part of the inelastic events. The fiducial cross-section is determined using a counting experiment, knowing the luminosity, trigger and selection efficiencies. The result is $\sigma_{\text{inel}}(\xi > 10^{-6}) = 68.1 \pm 0.6(exp) \pm 1.3(lumi)$ mb.

The total inelastic cross-section is determined by extrapolating the measured value to full phase space $\sigma_{\text{inel}} = 79.3 \pm 0.6(exp) \pm 1.3(lumi) \pm 2.5(extr)$ mb. Figure 3 shows how this measurement (labelled as "ATLAS (MBTS)") compares to the measurements at different energies and to various model predictions.

3. Charged-particle distributions

Going further into details of the hadronic interactions, the ATLAS Collaboration measured the inclusive charged-particle distributions for the inelastic events [6]. This measurement was performed at $\sqrt{s} = 13$ TeV. It is important to measure such distributions since they provide insight into the strong interaction in the non-perturbative QCD regime. Moreover, these distributions are used to obtain the MC generator tunes for the pile-up simulation.

The tracks are required to have $p_T > 500$ MeV and $|\eta| < 2.5$, and it is required to find at least one such track in the event. About 9 million of events passing the above selection have been collected in the special runs with low activity from additional pp interactions. The distributions are corrected for the trigger, vertex and tracking inefficiencies as well as for small background contribution, and the unfolding for the detector resolution effects was performed. The systematic uncertainties are generally dominated by the tracking efficiency uncertainty and are typically at the level of 1%–2% but up to 30%–50% for $n_{ch} > 130$.

Figure 4(a) presents the charged-particle multiplicity distribution. It is compared to various MC generators which vary in the simulation of the hard and soft processes and the way how the diffraction events are handled. The PYTHIA8 A2 tune [7, 8] provides a really good description up to $n_{ch} \simeq 60$ while the PYTHIA8 Monash tune [9] and EPOS [10] are performing reasonably well across the whole spectrum. The charge multiplicity as a function of the pseudorapidity (Fig. 4(b)) and the transverse momentum of the particles (Fig. 4(c)) are best described by the EPOS generator while PYTHIA8 A2/Monash tunes describe the data also relatively well. In Fig. 4(d), the average particle p_T is presented. A slow rise in $< p_T >$ is expected due to colour-reconnection effects. EPOS and PYTHIA8 Monash describe the data best while QGSJET [11] fails, because it has no model for the colour-reconnection effects. It should be noted that all of the tunes have been previously tuned to $\sqrt{s} = 7$ TeV LHC data. This shows that the extrapolation of particle production to the higher energy of interactions works quite well.

In Fig. 5, the average charged-particle density at zero pseudorapidity is presented for different centre-or-mass energies. There is about 20% increase in density going from $\sqrt{s} = 7$ TeV to $\sqrt{s} = 13$ TeV.

4. Underlying event distributions

The measurement of the distributions which are sensitive to the underlying event (UE) is also performed at $\sqrt{s} = 13$ TeV [12]. The underlying event is defined as any activity accompanying the hard scattering, e.g. the multi-parton interactions and the beam remnants. By measuring such distributions, the multi-parton interaction models in MC simulation can be constrained.

This analysis uses the same dataset and follows the same event and track selections as the analysis measuring the charged-particle distributions above. Additionally, it applies a cut on the momentum of the leading charged particle p_T^{lead}, either 1 GeV or 5 GeV.

The direction of the leading track is used to define regions in the azimuthal plane that have different sensitivity to the UE, see Fig. 6. Three different regions are defined. The transverse region is especially sensitive to underlying event, since the particles from the hard scattering are usually flying in toward and away region.

The measured distributions are not corrected for the detector efficiency and the resolution effects. The average track density and average scalar sum p_T density of tracks are measured as a function of difference between the track and leading track in the azimuthal angle, see Fig. 7. For the higher cut on p_T^{lead}, the jet-like structure in the toward region and a little bit less in the away region can be observed. There is about constant activity in the transverse region. The MC generators agree quite well with the data, especially in the higher-p_T region.
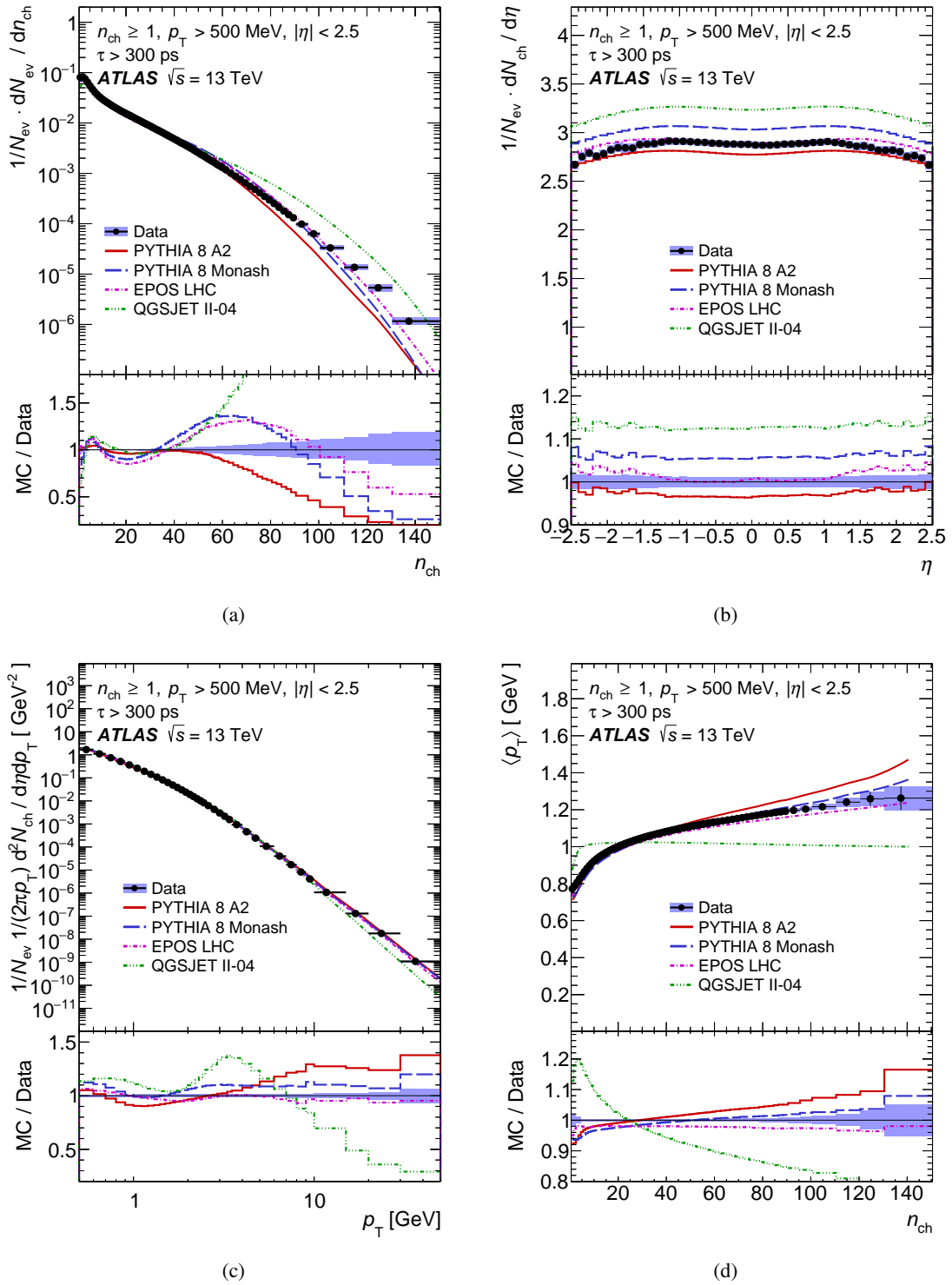
Figure 4: The primary charged-particle multiplicity distribution (a), the multiplicity as a function of (b) pseudorapidity, and (c) transverse momentum; and (d) the mean transverse momentum, $< p_T >$, versus particle multiplicity [6].
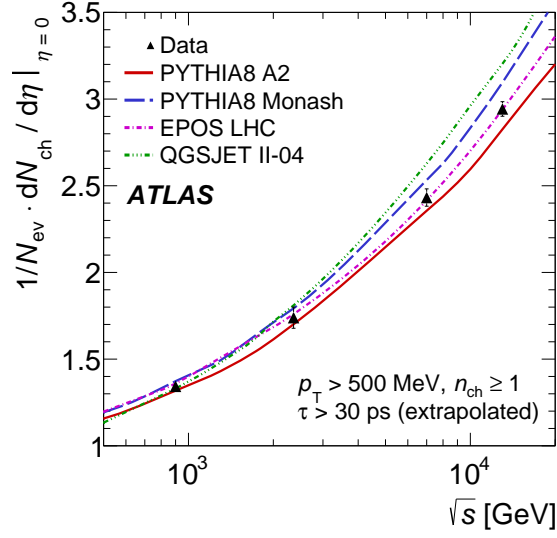
Figure 5: The average primary charged-particle multiplicity in *pp* interactions per unit of pseudorapidity for $|\eta| < 0.2$ as a function of the centre-of-mass energy [6].
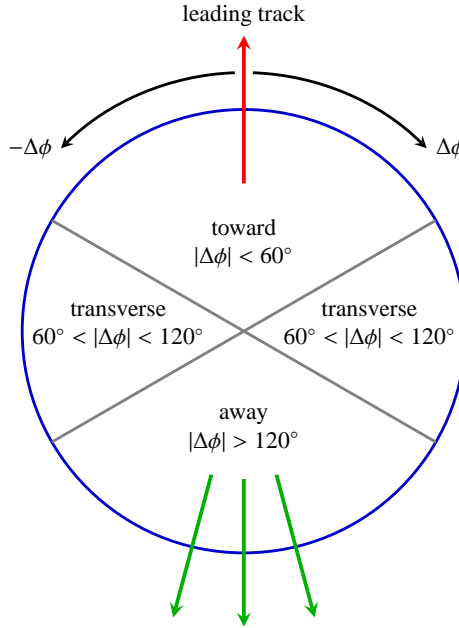

Figure 6: Definition of UE regions as a function of the azimuthal angle with respect to the leading track [12].

The same particle densities as above are measured as a function of p_T^{lead}, see Fig. 8. In the transverse region, there is a plateau starting at $p_T^{lead} \sim 6$ GeV. In the toward region, the behaviour is quite different due to hard process contributions.

The increase in UE activity is about 20% compared to $\sqrt{s} = 7$ TeV. Most of the MC generators agree well with the data, which gives some confidence in the energy extrapolation of the multi-parton interaction models from $\sqrt{s} = 7$ TeV to $\sqrt{s} = 13$ TeV.
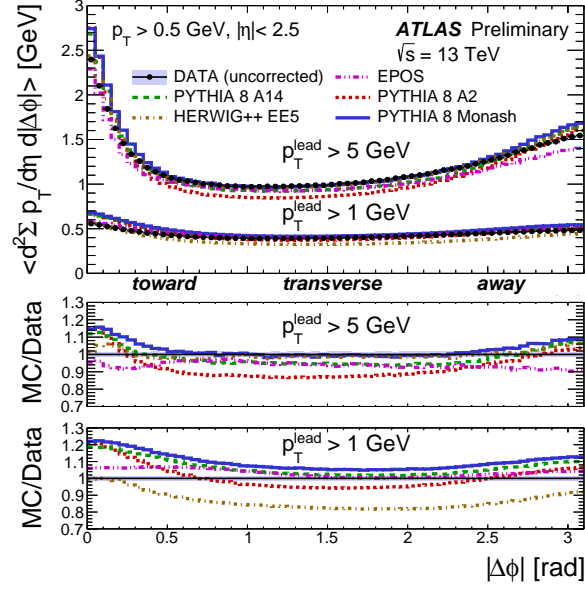
Figure 7: Comparison of detector level data and MC predictions for the $|\Delta\phi|$ distributions of average scalar $p_{\rm T}$ sum density of tracks [12].
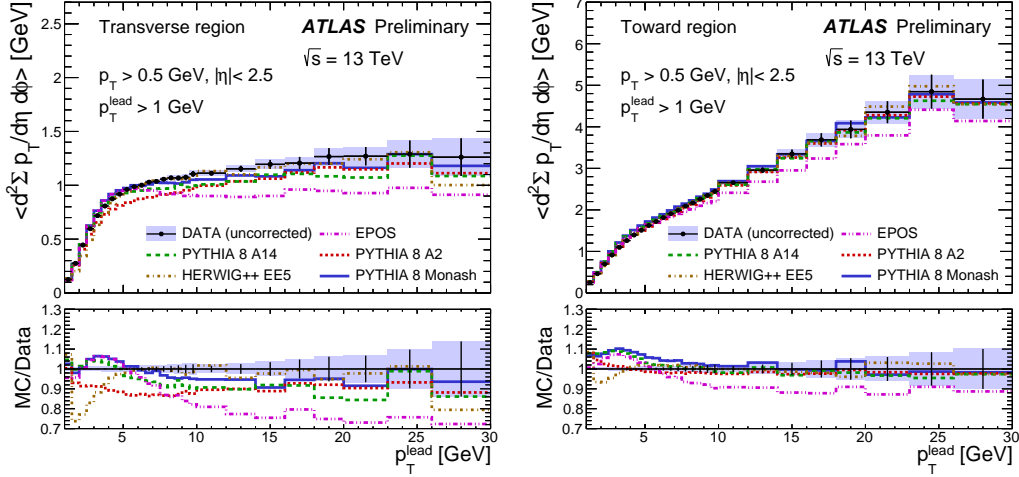

Figure 8: Comparison of detector level data and MC predictions for average scalar $p_{\rm T}$ sum density of tracks as a function of leading track transverse momentum, $p_{\rm T}^{\rm lead}$, in the transverse (left) and toward (right) regions [12].

5. Diffractive dijet production

The properties of the inelastic events have been studied in previous measurements in Sec. 3 and Sec. 4. The large fraction ($\sim 20\%$) of the inelastic events are diffractive processes. The specific subcategory of such events is studied where a colour-less object emits a parton and together with a parton coming directly from the other proton produces a pair of jets, see Fig. 9 for the most contributing diagram of such process. Such events are sensitive to parton dynamics of diffraction

and colour-singlet exchange. This measurement was performed at $\sqrt{s} = 7$ TeV [13].
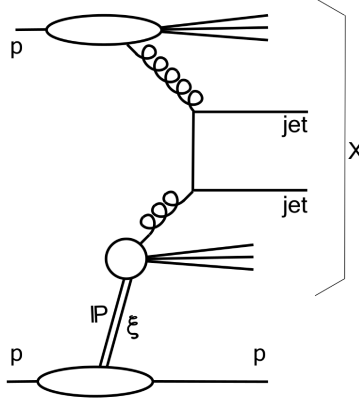

Figure 9: Illustration of hard single-diffractive scattering, in which partons from a pomeron (IP) and from a proton enter a hard sub-process. The rapidity gap $\Delta\eta_F$ appears between the system X and the intact proton [13].

At least two high-p_{T} jets with $p_{\mathrm{T}} > 20$ GeV and $|\eta| < 4.4$ are required in the final state. The jets are reconstructed with the anti-k_t algorithm with two different radius parameters $R = 0.4$ and $R = 0.6$. The differential cross-section as a function of two variables is measured. These variables are able to separate the diffractive and non-diffractive (ND) events: the size of the rapidity gap which is devoid of hadronic activity within the ATLAS detector acceptance range of $|\eta| < 4.8$, $\Delta\eta_F$, and the fractional momentum loss of intact proton $\xi \simeq M_X^2/s$, where M_X is the invariant mass of the dissociative system, see Fig. 10. The region of high $\Delta\eta_F$ is completely dominated by diffractive processes similarly to low region of ξ. The data are well described by PYTHIA8 MC generator which includes single (SD) and double (DD) diffractive processes. The overall systematic uncertainty varies in the range of 20%–50%, where the dominant uncertainty arises from the jet energy scale uncertainty.

The leading order POMWIG MC generator is based on standard implementation of the hard diffractive scattering including factorizable pomeron and diffractive parton distribution functions. The rapidity-gap survival probability appropriate to the mixed POMWIG/ PYTHIA8 ND model is estimated by taking the ratio of the measured cross-section after removing the ND and DD contributions, and the SD POMWIG prediction in the region dominated by the diffractive events, i.e. where $\Delta\eta_F > 2$ and $-3.2 < \log_{10}\xi < 2.5$, see Fig. 10. The result is $S^2 = 0.16 \pm 0.04(stat) \pm 0.08(syst)$, where the dominant systematic uncertainties are due to uncertainties in ND and DD contributions.

6. Exclusive diphoton production of dileptons

Another specific subcategory of soft processes is the exclusive diphoton production of two leptons $\gamma + \gamma \to \ell\ell$, where the interacting protons stay intact in the final state and the quasi-real photons emitted by the protons interact and produce the dilepton pair, see Fig. 11. The diphoton production is the quantum electrodynamic process and so it is predicted very precisely ($< 2\%$).
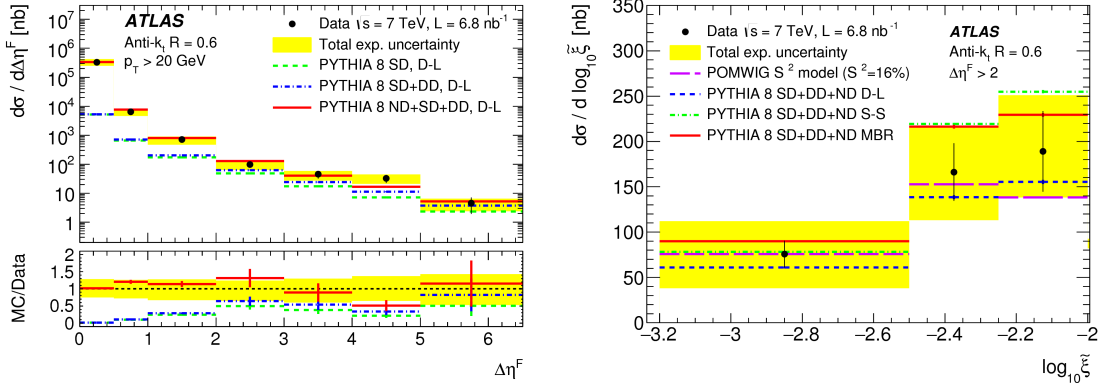
Figure 10: The differential dijet cross-section as a function of $\Delta\eta_F$ (left), compared with the PYTHIA8 model where the different diffractive contributions are included. The Donnachie–Landshoff pomeron flux model is used for the diffractive components. The differential cross-section as a function of ξ (right) for the events satisfying $\Delta\eta_F > 2$. The 'POMWIG S2' model represents the sum of PYTHIA ND and POMWIG, with POMWIG multiplied by 0.16 [13].
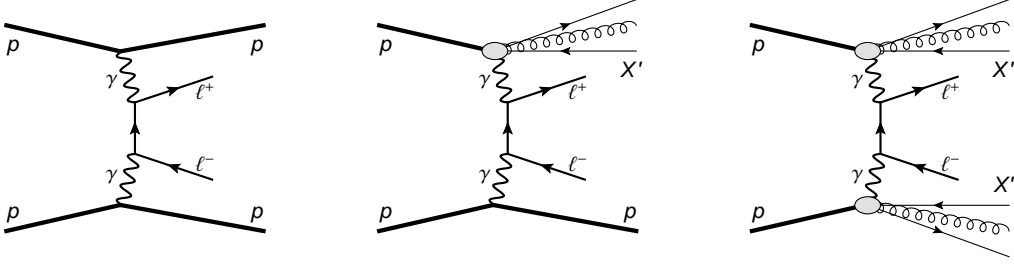

Figure 11: Schematic diagrams for exclusive (left), single-proton dissociative (middle) and double-proton dissociative (right) two-photon production of lepton pairs in pp collisions [14].

The fiducial cross-section of $\gamma + \gamma \rightarrow \ell\ell$ process has been measured at $\sqrt{s} = 7$ TeV [14]. Two electrons (muons) with $p_T > 12(10)$ GeV and $m_{\ell\ell} > 24(20)$ GeV are required and any other activity is vetoed in the central detector. The dominant background processes are similar to the signal but have at least one dissociated proton in the final state, see Fig 11. The acoplanarity distribution, which is closely related to the difference in the azimuthal angle of the leptons, has been used to distinguish between the signal and the background, see Fig. 12. The template fit to such distribution has been performed and the fiducial cross-sections has been obtained. The statistical uncertainties are about twice as large as the systematic uncertainties which are about 3%–4% and are dominated by the background modeling uncertainty. The measured cross-sections are about 20% smaller when compared to the theoretical predictions based on the nominal equivalent photon approximation (EPA), see Fig. 12. When the proton absorptive effects due to finite proton size are taken into account, the predictions agree well with the data.

7. Conclusions

The initial ATLAS soft QCD measurements from LHC Run 2 together with the recent results from LHC Run 1 have been presented. Many more results are being prepared with the up-to date
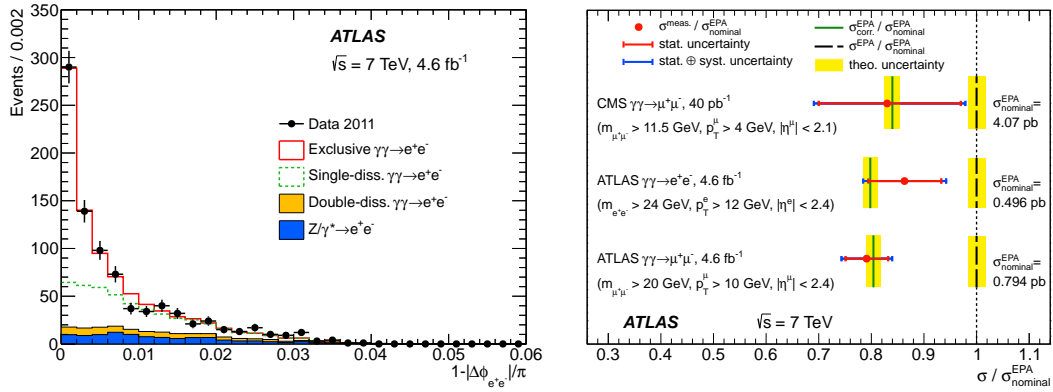
Figure 12: Di-electron acoplanarity distribution (left) after the selection requirements. The exclusive and single-dissociative yields are determined from the fit. On right, comparison of the ratios of measured (red points) and predicted (solid green lines) cross-sections to the uncorrected EPA calculations (black dashed lines). Results for the muon and electron channels are also compared with a similar CMS measurement. The yellow band represents the theoretical uncertainty of 1.8% (1.7%) on the predicted (uncorrected EPA) cross-section [14].

list of the measurements being available at the ATLAS public web page [15].

References

[1] ATLAS Collaboration, JINST **3** (2008) S08003.

[2] ATLAS Collaboration, Nucl. Phys. B **889** (2014) 486, arXiv:1408.5778 [hep-ex].

[3] J. R. Cudell *et al.* (COMPETE Collaboration), Phys. Rev. Lett. **89** (2002) 201801, arXiv:hep-ph/0206172.

[4] G. Antchev *et al.* (TOTEM Collaboration), Europhys. Lett. **101** (2013) 21002.

[5] ATLAS Collaboration, arXiv:1606.02625 [hep-ex].

[6] ATLAS Collaboration, Phys. Lett. B **758** (2016) 67, arXiv:1602.01633 [hep-ex].

[7] T. Sjostrand, S. Mrenna and P. Z. Skands, Comput. Phys. Commun. **178** (2008) 852, arXiv:0710.3820 [hep-ph].

[8] ATLAS Collaboration, ATL-PHYS-PUB-2011-014, http://cds.cern.ch/record/1400677.

[9] P. Skands, S. Carrazza and J. Rojo, Eur. Phys. J. C **74** (2014) no.8, 3024, arXiv:1404.5630 [hep-ph].

[10] S. Porteboeuf, T. Pierog and K. Werner, arXiv:1006.2967 [hep-ph].

[11] S. Ostapchenko, Phys. Rev. D **83** (2011) 014018, arXiv:1010.1869 [hep-ph].

[12] ATLAS Collaboration, ATL-PHYS-PUB-2015-019, http://cds.cern.ch/record/2037684.

[13] ATLAS Collaboration, Phys. Lett. B **754** (2016) 214, arXiv:1511.00502 [hep-ex].

[14] ATLAS Collaboration, Phys. Lett. B **749** (2015) 242, arXiv:1506.07098 [hep-ex].

[15] ATLAS Collaboration, ATLAS Experiment – Public Results, Soft QCD public results, https://twiki.cern.ch/twiki/bin/view/AtlasPublic/StandardModelPublicResults#Soft_QCD